Nuclear Structure of Manganese-56*†

J. R. COMFORT
Wright Nuclear Structure Laboratory, Yale University, New Haven, Connecticut 06511

(Received 19 June 1968)

The $Mn^{55}(d, p)Mn^{56}$ reaction was investigated with 10-keV resolution at a deuteron bombarding energy of 7.5 MeV. Angular distributions were obtained for most states up to 5.5 MeV and for strong states up to about 6.5 MeV of excitation energy. A distorted-wave (DW) analysis yielded the orbital angular momentum transfer l_n and the transition strength $(2J_f+1)S_{lj}$ for most states. A comparison with the (d, p) sum rules gives evidence that the DW calculations may be accurate to about 20%. Considerable configuration mixing between the $2p_{3/2}$, $2p_{1/2}$, and $1f_{5/2}$ neutron orbitals was found. A discussion of possible spin assignments is given, particularly for states below 1 MeV. The statistical model is found to be reasonably consistent with the present data, but the distribution of nearest-neighbor spacings has some features of a Wigner, and not an exponential, distribution. Shell-model calculations are discussed, and the possibility that Mn^{56} may have a large static deformation is considered.

I. INTRODUCTION

THE present work is largely intended to be a detailed spectroscopic study of the odd-odd nucleus Mn^{56} as it is seen with the $Mn^{55}(d, p)Mn^{56}$ reaction. The spectrum is investigated over the excitation region between the ground state and the neutron binding energy of 7.28 MeV. Angular distributions are obtained for a large number of states below 6.6 MeV of excitation energy.

Although many experimental and theoretical studies have been made on nuclei in the $1f$-$2p$ shell region of the periodic table, very few have been directed to Mn^{56} in particular. The complexity of its spectrum has made it a very difficult nucleus for detailed study. Nevertheless, this very characteristic makes it a very favorable nucleus for a more qualitative investigation of the nuclear Hamiltonian. The large number of states, many of which are individually resolvable, allows reasonable comparisons to be made with the statistical model concerning their number, density, and nearest-neighbor spacings.

Of even greater importance is the distribution of neutron single-particle strength in the spectrum. The fragmentation of this strength into many individual states can be observed, and the envelope can be traced over a wide range of excitation energy. In particular, the favorable cross sections and distinctive angular distributions associated with $l_n=1$ transfer allow the single-particle p neutron strength to be examined in detail. Systematic studies of single-particle transfer reactions[1] have suggested that the $2p$ strength is centered near 1–2 MeV, with the $3p$ strength located at much higher excitation energies. However, previous experiments on $1f$-$2p$ nuclei have not been able to determine the distribution of p strength sufficiently well to ascertain whether the $2p$ and $3p$ strengths might overlap significantly at high excitations. From such information one may hope to obtain significant information concerning the nature and complexity of the residual interactions.

The $1f$-$2p$ shell region continues to be an especially interesting region of the periodic table. It has often been considered to be a region that is particularly tractable to description by the spherical shell model. Many calculations have been made with this model,[2–5] and the results have been reasonably successful. Recently, alternative calculations have been made with the strong-coupling, symmetric-rotator model with Coriolis coupling and a Nilsson basis.[6,7] Again, the results have been successful in interpreting the known properties of the odd-mass nuclei in this region and suggest that these nuclei may have large static deformations.

For any model, calculations of the Mn^{56} spectrum are made extremely difficult by the large number of states and the complexity of their wave functions. The low-lying states are expected to have configurations characterized by five protons in the $1f_{7/2}$ orbital and three neutrons in the $2p_{3/2}$-$1f_{5/2}$ orbitals. The few available calculations for odd-odd nuclei in this region[2,3,8] have been limited to cases with less complicated configurations. Techniques are being developed for treating odd-odd nuclei within the framework of either the pairing model[9] or the deformed Nilsson model with Coriolis coupling.[10–12]

* Supported in part by the U.S. Atomic Energy Commission under Contract No. AT(30-1)-3223.

† Portions of this work were submitted by the author to the Graduate School of Yale University in partial fulfillment of the requirements for the Ph.D. degree.

[1] B. L. Cohen, Phys. Rev. **130**, 227 (1963).

[2] J. D. McCullen, B. F. Bayman, and L. Zamick, Phys. Rev. **134**, B515 (1964).

[3] J. Vervier, Nucl. Phys. **78**, 497 (1966).

[4] S. Cohen, R. D. Lawson, M. H. Macfarlane, S. P. Pandya, and M. Soga, Phys. Rev. **160**, 903 (1967).

[5] J. B. McGrory, Phys. Rev. **160**, 915 (1967).

[6] W. Scholz and F. B. Malik, Phys. Rev. **147**, 836 (1966).

[7] F. B. Malik and W. Scholz, Phys. Rev. **150**, 919 (1966).

[8] H. U. Gersch, C. Riedel, and W. Rudolph, Nucl. Phys. **A97**, 65 (1967).

[9] L. S. Kisslinger and D. M. Rote, Phys. Rev. Letters **16**, 659 (1966).

[10] C. Daum, Nucl. Phys. **51**, 244 (1964).

[11] H. T. Motz *et al.*, Phys. Rev. **155**, 1265 (1967).

[12] P. Wasielewski, Bull. Am. Phys. Soc. **13**, 723 (1968); and private communication.

This study has also been motivated by a desire to study reaction mechanisms and, in particular, to compare the transition strengths for the $Mn^{55}(d, p)Mn^{56}$ and $Mn^{55}(n, \gamma)Mn^{56}$ reactions. This aspect has been discussed in an earlier publication.[13] In the present paper, the observation of the single-particle strength over a wide range of excitation energy is used to check the accuracy of the distorted-wave (DW) calculations against theoretical sum rules, assuming that all of the available strength is observed and correctly assigned and that the ground-state configuration of the target nucleus is known.

Limited information has been obtained on the $Mn^{55}(d, p)Mn^{56}$ reaction in earlier studies. The total (d, p) excitation function has been studied with activation techniques in large energy steps between 4.5 and 11.6 MeV.[14] The energies of many states below 5.6 MeV of excitation energy were determined with a single-gap magnetic spectrograph,[15] but no angular distributions were obtained. Schiffer *et al.*[16] made angular distribution measurements with very broad energy resolution in order to study the gross structure of the (d, p) spectrum and perhaps determine the location of the shell-model orbitals. A more detailed study of the (d, p) angular distributions was made by Dalton *et al.*[17] with 8.9-MeV deuterons and about 50-keV resolution. Unfortunately, this study could not separate all of the states, even at low excitation energy (the first excited state is at 25 keV), and the analysis suffered from a plane-wave treatment of the reaction mechanism. The present data were obtained with a multiple-gap magnetic spectrograph so that high-resolution spectra at many angles could be obtained simultaneously. In this way, many of the limitations inherent in the previous studies have been overcome.

II. EXPERIMENTAL PROCEDURES

A. Data Acquisition

The data for this experiment were obtained at the Massachusetts Institute of Technology. The target consisted of a thin Mn^{55} film evaporated onto a Formvar backing.[18] This target was remarkably clean. Apart from the carbon and oxygen in the backing, the only contaminants which could be identified from the data were negligible traces of N^{14}, Si^{28}, and S^{32}.

The target was bombarded with 7.5-MeV deuterons from the MIT-ONR Van de Graaff accelerator. The reaction protons were momentum-analyzed in the MIT multigap magnetic spectrograph.[19] Spectra were obtained at 24 angles from 7.5° to 172.5° in 7.5° intervals. The protons were detected with 50-μ Kodak NTA nuclear emulsions. These were covered with $2\frac{1}{2}$ mils of aluminum to prevent all other reaction products from being recorded.

The spectrum of Mn^{56} was obtained in two separate exposures employing different magnetic fields in the spectrograph. The first spanned the excitation region between the ground state and about 6 MeV. The second spanned the region between about 3.5 and about 8.5 MeV. In this way, a much larger region of excitation energy could be investigated. In addition, a more accurate analysis of the spectrum at higher excitations could be made on the second exposure, since that portion was moved along the focal plane to a region of larger dispersion.

A short exposure of the low-excitation region of Mn^{56} was made on a separate target for the purpose of normalizing the main (d, p) exposures. The thickness of this target (34 $\mu g/cm^2$) was determined by elastically scattering 2.56-MeV deuterons from the Mn^{55} and assuming that the cross section could be described by the Rutherford law. Finally, an exposure of the elastic scattering of 7.5-MeV deuterons from Mn^{55} was obtained from the same target. Absolute cross-section scales were calculated for all exposures. It is believed that these are accurate to within 5%–10%.

The developed emulsions were microscopically scanned in 0.5-mm-wide strips, i.e., about 4-keV channels. Typical spectra from the first and second main exposures are shown in Figs. 1 and 2, respectively. The over-all resolution was about 10 keV, as is illustrated by the clean separation of the ground and first excited states ($\Delta E = 25$ keV) in Fig. 1. The spectra at a very few angles had slightly inferior resolution and portions of them, particularly at high excitation energies, were discarded. The plates of the second exposure for angles larger than 90° were not scanned because of the inadequate yield from that exposure and the presence of strong carbon and oxygen peaks.

B. Data Analysis

Except for the easily identified carbon and oxygen states, there were very few contaminate peaks in the spectra and the identification of the Mn^{56} levels was relatively easy. It was impeded, however, by the extreme complexity of the spectra, especially at high excitation energies. All of the assignments were confirmed by a kinematic analysis of the data. For each angle the spectrum was plotted as counts versus reaction Q value (assuming a residual mass of 56) and the graphs were aligned vertically. The levels of Mn^{56} were observed to lie along vertical straight lines.

[13] J. R. Comfort, Phys. Rev. Letters **20**, 941 (1968), **21**, 1030 (E) (1968).
[14] L. J. Gilly, G. A. Henriet, M. Preciosa Alves, and P. C. Capron, Phys. Rev. **131**, 1727 (1963).
[15] J. W. Green, A. J. Smith, W. W. Buechner, and M. Mazari, Phys. Rev. **108**, 841 (1957).
[16] J. P. Schiffer, L. L. Lee, Jr., and B. Zeidman, Phys. Rev. **115**, 427 (1959).
[17] A. W. Dalton, G. Parry, H. D. Scott, and S. Swierszczewski, Proc. Phys. Soc. (London) **78**, 404 (1961).
[18] The target was kindly made available to us by the MIT group.
[19] H. A. Enge and W. W. Buechner, Rev. Sci. Instr. **34**, 155 (1963).

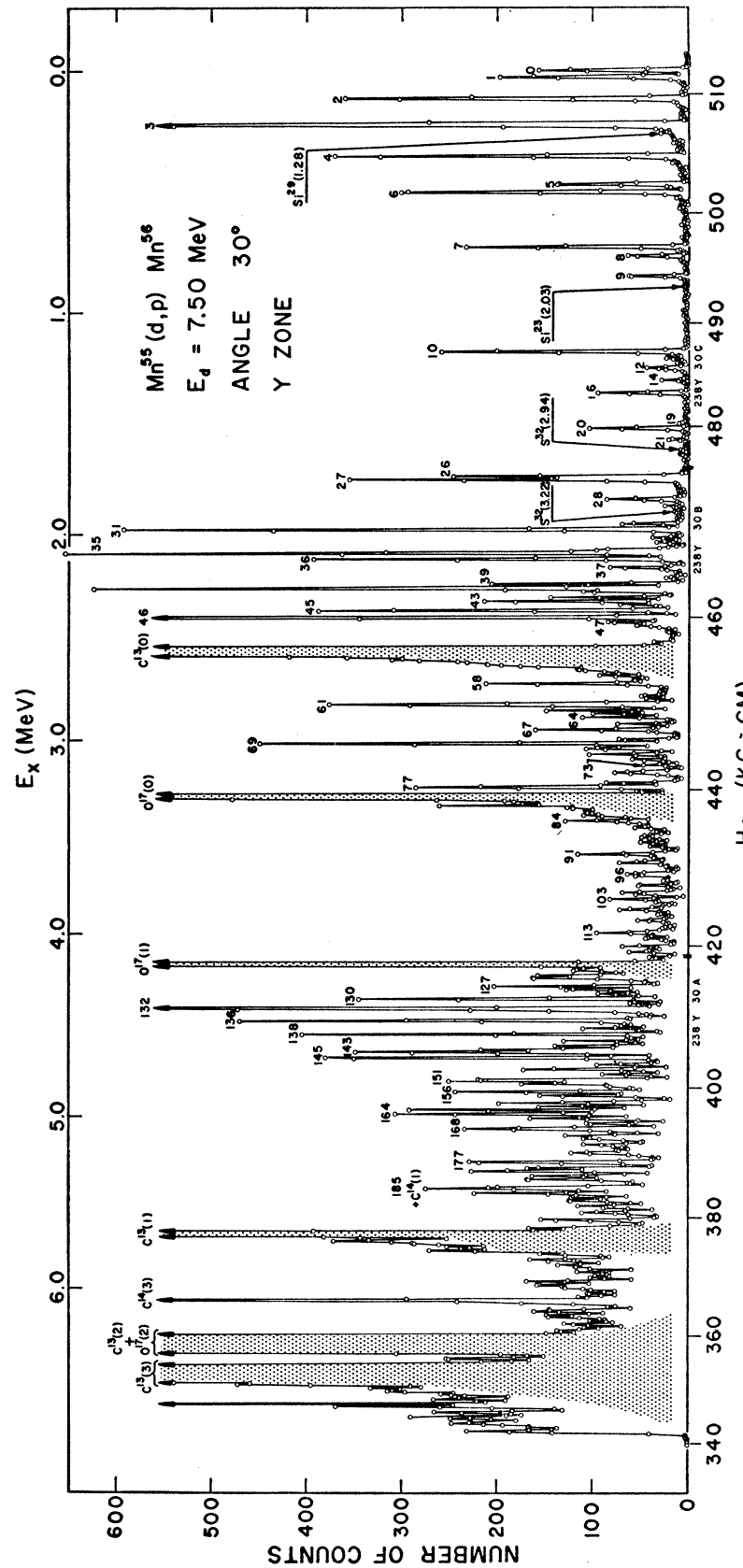

FIG. 1. Proton spectrum from the $Mn^{55}(d,p)Mn^{56}$ reaction at 30° for the first main exposure. The number of counts in each 0.5-mm-wide strip is shown plotted against magnetic rigidity along the bottom axis and excitation energy along the top axis. Numbers above the peaks identify the levels listed in Table III. Prominent carbon and oxygen peaks are shaded, and other contaminants are labeled.

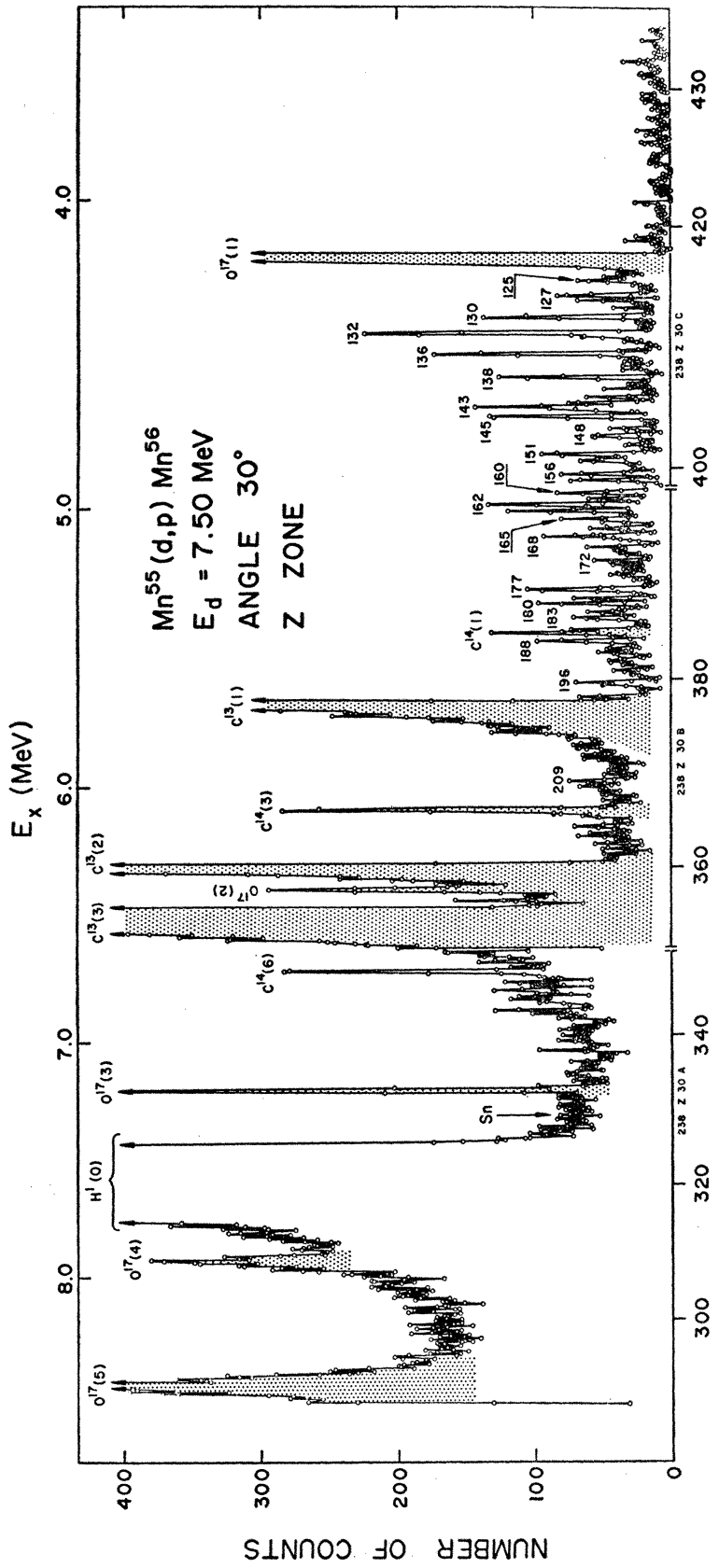

FIG. 2. Spectrum of the $Mn^{55}(d, p)Mn^{56}$ reaction at 30° for the second main exposure. See also the caption of Fig. 1.

In order to compensate for small effects of differential hysteresis in the MIT spectrograph, it was necessary to adopt a set of effective magnetic fields, a slightly different field for each gap. These were obtained by requiring that the Q values for several easily identified levels of Mn^{56} be consistent with those determined in the earlier MIT measurements of level positions.[15] No effective field differed by more than 0.11% from the value given by the monitor NMR probe. Further discussion may be found elsewhere.[20]

The exact locations and areas of the Mn^{56} peaks were determined with the use of the automatic spectrum decomposition computer program AUTOFIT written at the Argonne National Laboratory.[21] Although the program was fully capable of determining the areas of the peaks to an accuracy of a few percent in most cases, some of the results are limited in precision by the presence of backgrounds in the spectra. In the excitation region of the spectra below the occurrence of the contaminate C^{13} ground-state peak (near 2.5-MeV excitation), there are no backgrounds (except possibly at some back angles). Above that excitation energy, backgrounds result from the tails of the contaminate peaks. These are difficult to estimate. Furthermore, a large number of very weakly populated states can simulate a type of background which cannot be distinguished from the contaminate background. In this experiment, the backgrounds which were subtracted from the data were estimated by the lowest-lying data points between peaks in any given region. This may overestimate the cross sections of the high-lying states, but will automatically compensate for the strength of the unobserved levels. After inspection and editing, the results from program AUTOFIT were compiled to produce a list of reaction Q values and graphs of angular distributions for 211 states of Mn^{56}.

III. DW ANALYSIS

The angular distributions were analyzed with the DW Born approximation description of the reaction mechanism. The differential cross section is given by

$$d\sigma/d\Omega = 1.5[(2J_f+1)/(2J_i+1)]\sum_{lj} S_{lj}\sigma_{lj}(\theta), \quad (1)$$

where J_i and J_f are the angular momenta of the target nucleus and final state, respectively, and S_{lj} is the spectroscopic factor. The factor of 1.5 is associated with the use of a Hulthén wave function for the deuteron. The theoretical cross section for a single-particle transfer is contained in $\sigma_{lj}(\theta)$ and was computed with the Oak Ridge computer program JULIE.[22] All of these calculations used zero-range interactions and local potentials. Radial cutoffs were not found to be necessary and were not used.

The wave functions for the captured neutrons were calculated for a Woods-Saxon potential,

$$V_n(r) = -V_n\{1+\exp[(r-r_0A^{1/3})/a]\}^{-1} + \text{spin-orbit term.} \quad (2)$$

The wave functions for the deuteron and proton channels were obtained from optical potentials of the form

$$U(r) = -Vf(r, r_0, a) + i4a'W'(d/dr)f(r, r', a') + V_c(r, r_c), \quad (3)$$

where

$$f(r, r_0, a) = \{1+\exp[(r-r_0A^{1/3})/a]\}^{-1}. \quad (4)$$

V and W' are the well depths of the real and surface-derivative absorption potentials, respectively. V_c is the Coulomb potential resulting from a uniformly charged sphere of radius $R_c=r_cA^{1/3}$. A spin-orbit term of the Thomas form may be added to the potential $U(r)$. The effects of such a term were found to be negligible in both the proton and deuteron channels. It was used only in the proton potential for states below 1.25 MeV of excitation energy.

A. Selection of Parameters

Numerous sets of parameters were investigated in an effort to obtain the best DW calculations for the angular distributions. A complete list of all of the parameter sets tested is given in Table I. A full description of the investigations is given elsewhere.[20]

The geometrical parameters for the neutron potential were taken from the work of Bjorklund and Fernbach.[23] The well depth V_n was adjusted by program JULIE to reproduce the observed binding energy for each state. Some authors[24] have suggested that a value $r_0=1.20$ may be more appropriate for the radius parameter. It was found here that such a value did not change the shapes of the calculated (d, p) angular distributions, but decreased the cross sections by about 10–15%.

The proton parameter sets in Table I were obtained from various studies of proton elastic scattering[25–27] and polarization[28] data. Optical-model calculations obtained with each set were compared against good-quality data[26,28] in the mass and energy region relevant to this experiment. Parameter set RA was selected for use in the DW calculations on the basis of its ability to reproduce elastic scattering data at least as well as the other parameter sets, and for its superiority in repro-

[20] J. R. Comfort, Ph.D. thesis, Yale University, 1968 (unpublished).
[21] P. Spink and J. R. Erskine, Argonne National Laboratory Physics Division Informal Report No. PHY-1965B, 1965 (unpublished), and private communication.
[22] R. H. Bassel, R. M. Drisko, and G. R. Satchler, Oak Ridge National Laboratory Report No. ORNL-3240, 1962, and Supplement, 1966 (unpublished), and private communication.
[23] F. Bjorklund and S. Fernbach, Phys. Rev. **109**, 1295 (1958).
[24] L. L. Lee, Jr., J. P. Schiffer, B. Zeidman, G. R. Satchler, R. M. Drisko, and R. H. Bassel, Phys. Rev. **136**, B971 (1964).
[25] F. G. Perey, Phys. Rev. **131**, 745 (1963).
[26] L. L. Lee, Jr., and J. P. Schiffer, Phys. Rev. **134**, B765 (1964).
[27] A. Marinov, L. L. Lee, Jr., and J. P. Schiffer, Phys. Rev. **145**, 852 (1966).
[28] L. Rosen, J. G. Beery, A. S. Goldhaber, and E. H. Auerbach, Ann. Phys. (N.Y.) **34**, 96 (1965).

TABLE I. Optical-model potential parameter sets investigated in the present study. Lengths are in fermis and well depths are in MeV. For deuteron potentials, the χ^2 goodness-of-fit criterion is also given. These values are normalized by a $1/N$ factor, where N is the number of data points.

Set	V	r_0	a	W'	r'	a'	V_{so}	r_c	χ^2
Neutrons									
BF[a]	b	1.25	0.65						
Protons									
P0	(51.9)[c,d]	1.25	0.65	13.5	1.25	0.47	(7.5)[e]	1.30	
P1	(49.4)[c,f]	1.25	0.65	13.5	1.25	0.47	(7.5)[e]	1.30	
P2	(49.4)[c,f]	1.25	0.65	12.2	1.25	0.47	(7.5)[e]	1.30	
LS	(52.0)[c,g]	1.25	0.65	12.2	1.25	0.47	(7.5)[e]	1.25	
RA[a]	(49.6)[c,h]	1.25	0.65	7.5	1.25	0.70	5.5	1.25	
Deuterons									
PB0	91.0	1.15	0.81	18.0	1.34	0.68		1.15	6.1
PB1[a]	89.75	1.15	0.786	18.13	1.328	0.69		1.25	1.8
CA	110.0	1.00	0.838	13.47	1.366	0.76		1.25	2.4

[a] These potentials were used in the final DW calculations.
[b] Neutron well depth adjusted by program to yield experimental separation energies.
[c] Proton well depths quoted for 12.5-MeV protons on Mn^{56}, corresponding to those from the ground-state transition in the present work; functional dependence is given in Refs. d and f–h.
[d] $V=53.3+0.4Z/A^{1/3}+27(N-Z)/A-0.55E$ MeV.
[e] Spin-orbit potential not used in (d, p) calculations.
[f] $V=46.7+Z/A^{1/3}-0.32E$ MeV.
[g] $V=50.1+0.4Z/A^{1/3}+27(N-Z)/A-0.33E$ MeV.
[h] $V=47.7+0.4Z/A^{1/3}+26.2(N-Z)/A-0.33E$ MeV.

ducing the polarization data. Its only significant weakness is in its predictions of proton total reaction cross sections. These are systematically higher than recent experimental values,[29] in contrast to the other potentials. It is only fair to note, however, that the (d, p) calculations are not especially sensitive to the particular choice of the proton potential. A change from set RA to set P1 would not significantly alter the shapes of the curves and would change the spectroscopic factors by less than 10%.

For the deuteron potential, parameter set PB0 was taken from the systematic study of deuteron elastic scattering by Perey and Perey.[30] Of the six parameter sets listed in that study only the set B has parameters which are near the values expected from theoretical considerations.[31,32]

The elastic scattering of 7.5-MeV deuterons from Mn^{55} was calculated with set PB0 and compared with the data obtained in the present study. Although the fit to the data was good, it was found that a better fit could be obtained if the parameters were varied slightly. This was accomplished by submitting the data to the automatic parameter search program ABACUS-II.[33] The parameter r_0 was held constant by the program at the value of 1.15 F. It was found that the χ^2 was very sensitive to small changes in the parameters a and r'. A much-improved fit to the data was obtained with set PB1 of Table I. Finally, an alternative set of parameters was obtained with the ABACUS-II program with r_0 held constant at 1.00 F. This is listed as set CA.

The data are compared with the optical-model

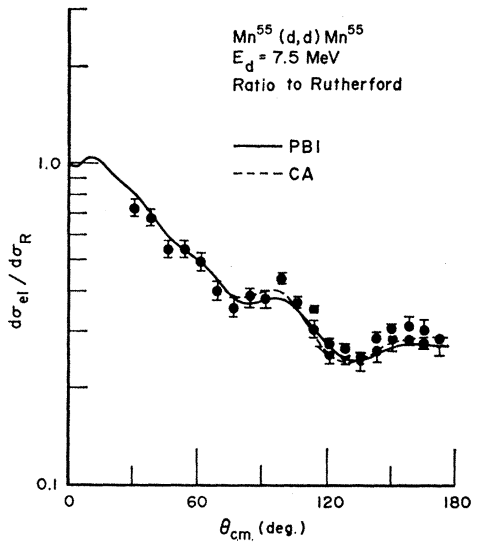

FIG. 3. Elastic deuteron scattering from Mn^{55}. Optical-model curves for parameter sets PB1 and CA of Table I are compared with experimental data. There are two sets of data at back angles.

[29] J. F. Dicello, G. J. Igo, and M. L. Roush, Phys. Rev. **157**, 1001 (1967).
[30] C. M. Perey and F. G. Perey, Phys. Rev. **132**, 755 (1963).
[31] J. R. Rook, Nucl. Phys. **61**, 219 (1965).
[32] J. Testori and L. C. Gomes, Nucl. Phys. **89**, 288 (1966).
[33] E. H. Auerbach (private communication).

calculations for parameter sets PB1 and CA in Fig. 3. There is little difference between the curves, although curve PB1 provides a smaller χ^2. Set PB1 was selected for use in the DW calculations largely because it had parameters very close to those of set PB0. The latter has successfully reproduced elastic scattering data throughout the periodic table for a wide range of deuteron energies.[30]

B. DW Calculations

In the present experiment, it was found that most transitions clearly required a mixture of two, or sometimes three, l_n values in the sum of Eq. (1). Conservation of parity limited the mixtures to either even values or odd values of l_n. An example of the latter is the ground-state transition. This is shown in Fig. 4. The bottom curve represents a pure $l_n=1$ transition, the middle curve represents equal admixtures of $l_n=1$ and $l_n=3$ components, and the top curve represents an $l_n=3$ mixture about 2.4 times that for $l_n=1$. The mixing of l_n values implies considerable configuration mixing in the Mn^{56} states, since, in most cases, the degree of mixing greatly exceeds the 5%–10% amount which could arise from higher-order stripping processes.[34–36]

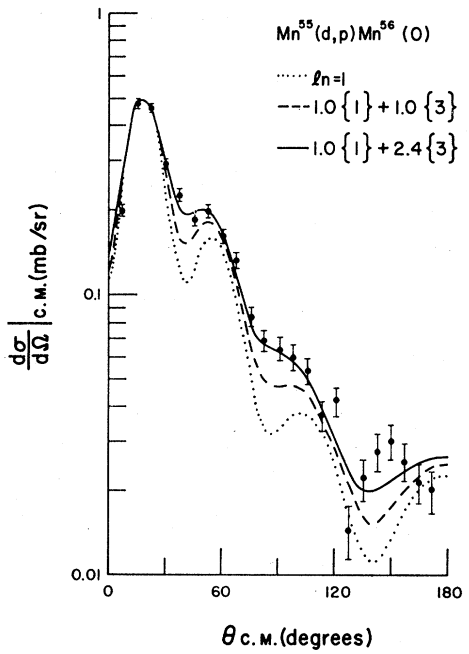

FIG. 4. The angular distribution for the Mn^{56} ground state compared with DW curves with various ratios of $l_n=1$ and $l_n=3$ components. The notation {1} means the DW curve for $l_n=1$, etc.

[34] F. S. Levin, Phys. Rev. **147**, 715 (1966).
[35] P. J. Iano and N. Austern, Phys. Rev. **151**, 853 (1966).
[36] S. K. Penny, Oak Ridge National Laboratory Report No. ORNL-TM-1414, 1966 (unpublished).

The experimental angular distributions were fitted in the following manner. First, a family of curves representing varying mixtures of the different l_n components was compiled. Then the curve which best fitted the shape of the angular distribution was selected and normalized to the data. All selections and normalizations were done visually, with emphasis given to the angular region before 90°. The fits obtained for the data are shown in Figs. 5–7. Only a small fraction of the available angular distributions are shown. A complete set may be obtained from the author.

The selection of the proper mixing ratio for each state was often subject to large uncertainties. Since the calculated cross sections $\sigma_{lj}(\theta)$ decreased rapidly as the value of l_n increased, the experimental angular distributions could easily retain the prominent features of a small value of l_n, even if the spectroscopic factor for a larger value of l_n was dominant. Thus the admixture of $l_n=3$ components in an angular distribution with $l_n=1$ features could not be determined very precisely and, in fact, admixtures of less than 25% were undetectable.

It is seen from the figures that the DW curves fit the data reasonably well, particularly for angles $\theta\leq 90°$. This arises partly from the fact that additional parameters are introduced by allowing curves for different values of l_n to mix. Fortunately, however, there were a number of transitions which did not require any mixtures of l_n values. These could be used to judge the suitability of the optical-model parameters for the DW calculations. In Figs. 5–7, these occur for states 2–4, 6, 8, 40, and 41. From these and the other examples (not shown), it was concluded that the parameters had been properly selected and that they were capable of reliably describing all of the available angular distributions.

There are, however, some systematic difficulties with the fits at the back angles. In general, the data points lie a little higher than the curves, particularly when the cross sections fall to values near 0.01 mb/sr. The reasons for this are not clear. There is evidence of residual backgrounds in the spectra at some of the back angles which could not be easily removed. It is also probable that compound-nucleus cross sections are becoming significant for the weaker states at these angles. Since the discrepancies are not large, we may conclude that the compound-nucleus processes do not significantly distort the spectroscopic information obtained with the DW calculations.

The reader may also have noticed another systematic difficulty at the back angles for some of the $l_n=1$ angular distributions For example, the data for states 2 and 3 show pronounced minima at the back angles and generally follow the DW curves, while the data for states 4 and 6 do not show such pronounced minima. Although this feature is reminiscent of the Lee-Schiffer dip arising from a j dependence in the (d, p) reaction

TABLE II. Changes in (d, p) transition strengths introduced by neutron spin-orbit, finite-range, and nonlocality effects. The upper portion lists the modifications required if a neutron spin-orbit potential of 25 times the Thomas term is used. The lower portion lists corrections for a finite-range n-p interaction and nonlocality effects in the neutron, proton, and deuteron potentials.

l_n	E_x (MeV)	$j_n=l_n+\frac{1}{2}$ (%)	$j_n=l_n-\frac{1}{2}$ (%)
1	1.0	−3	+6
1	3.5	−2	+5
2	1.5	−7	+12
3	2.0	−15	+24
4	2.5	−23	+45
5	3.0	−29	+57

l_n	E_x (MeV)	Finite range (%)	Nonlocality (%)
1	0.0	−3	−22
1	4.303	−2	−17
3	0.0	−1	−15
3	4.303	−3	−22

mechanism,[37,38] we do not believe that this is the correct explanation. The strongest argument against it is that the second excited state has[39] spin and parity $J^\pi=1^+$ and can be populated only with a $j_n=\frac{3}{2}$ transition. However, all previous observations of the $l_n=1$ j dependence show that the $j_n=\frac{1}{2}$ transitions have minima at back angles.[37,38] It must also be remembered that the back-angle data may include backgrounds or possible compound-nucleus contributions.

C. Corrections to DW Calculations

It was mentioned before that all calculations were made without radial cutoffs or neutron spin-orbit coupling and with local potentials and a zero-range n-p interaction. It is possible to estimate the corrections to be applied to the spectroscopic factors when these restrictions are removed.

The neutron spin-orbit term can raise serious problems. Its inclusion does not significantly change the shapes of the calculated angular distributions, but can result in large changes in their magnitudes. Since one does not usually know the value of $j_n=l_n\pm\frac{1}{2}$ that is transferred in a transition, the spin-orbit term cannot be included. Table II lists the corrections which must be applied to the values of the transition strengths. These are based on a neutron spin-orbit strength of 25 times the Thomas term. It must be borne in mind that, in the present experiment, both values of j_n, for a given l_n, may contribute to a single transition. Since the degree of mixing cannot be determined, the numbers in Table II represent upper limits to the corrections.

Estimates of the finite-range and nonlocality corrections were obtained with the Oak Ridge computer program FANLER,[40] in which use is made of the local-energy approximation.[41,42] A Gaussian function with a range of $R=1.25$ F was used for the n-p interaction. Nonlocality ranges were $\beta=0.85$ F for neutrons and protons and $\beta=0.54$ F for deuterons. Table II lists representative values of the corrections which should be applied to the transition strengths derived in the zero-range and local approximations.

D. Final Results

A full tabulation of the results of the DW analysis is given in Table III. For completeness, the table lists a few energy levels seen in the (n, γ) reaction[43] up to 4.0 MeV, but not definitely identified in the present (d, p) measurements. Level 10a may be the same as level 11, but it has been listed separately, because its energy is outside of the error limits allowed by the (n, γ) and (d, p) measurements. A number of levels could clearly be recognized as having two or more components. Although the individual components could not be reliably separated, they have been given separate level numbers in the table. In addition, levels 67, 79, 110, 117, 140, and 147 may also be doublets. Table IV lists the spectroscopic factors S_l for the lowest few states whose spins are known.

The Q value for the ground-state transition was calculated to be $Q_0=5.050$ MeV. This is 3-keV larger than the original MIT value,[15] and shows the typical agreement between the present and MIT Q values. The uncertainty in the present Q-value scale is believed to be less than 5 keV. Relative excitation energies are believed to be known to within 5 keV below 3 MeV, to within 8 keV below 5 MeV, and to within 10 keV above 5 MeV.

It is very difficult to assess the uncertainties which should be attached to the measurements of the transition strengths. In other papers, the reliability of DW calculations has been quoted to be anywhere between 20%[24] and a factor of 2.[44] The problems are enhanced in this experiment by the extensive mixing of l_n values in the angular distributions. Because of the weaker cross sections, the transition strengths for the larger values of l_n are usually determined less reliably than those for the small values. Evidence will be presented in Sec. IV that the present DW calculations are possibly

[37] L. L. Lee, Jr., and J. P. Schiffer, Phys. Rev. **136**, B405 (1964).
[38] L. L. Lee, Jr., and J. P. Schiffer, Phys. Rev. Letters **12**, 108 (1964).
[39] *Nuclear Data Sheets*, compiled by K. Way *et al.* (Printing and Publishing Office, National Academy of Sciences–National Research Council, Washington, D.C. 20025), NRC 59-4-52.
[40] J. K. Dickens and F. G. Perey, Oak Ridge National Laboratory Report No. ORNL-3858, 1965, Vol. 1, p. 49 (unpublished), and private communication.
[41] F. G. Perey and D. S. Saxon, Phys. Letters **10**, 107 (1964).
[42] J. K. Dickens, R. M. Drisko, F. G. Perey, and G. R. Satchler, Phys. Letters **15**, 337 (1965).
[43] L. B. Hughes, T. J. Kennett, and W. V. Prestwich, Nucl. Phys. **80**, 131 (1966).
[44] W. R. Smith, Phys. Rev. **137**, B913 (1965).

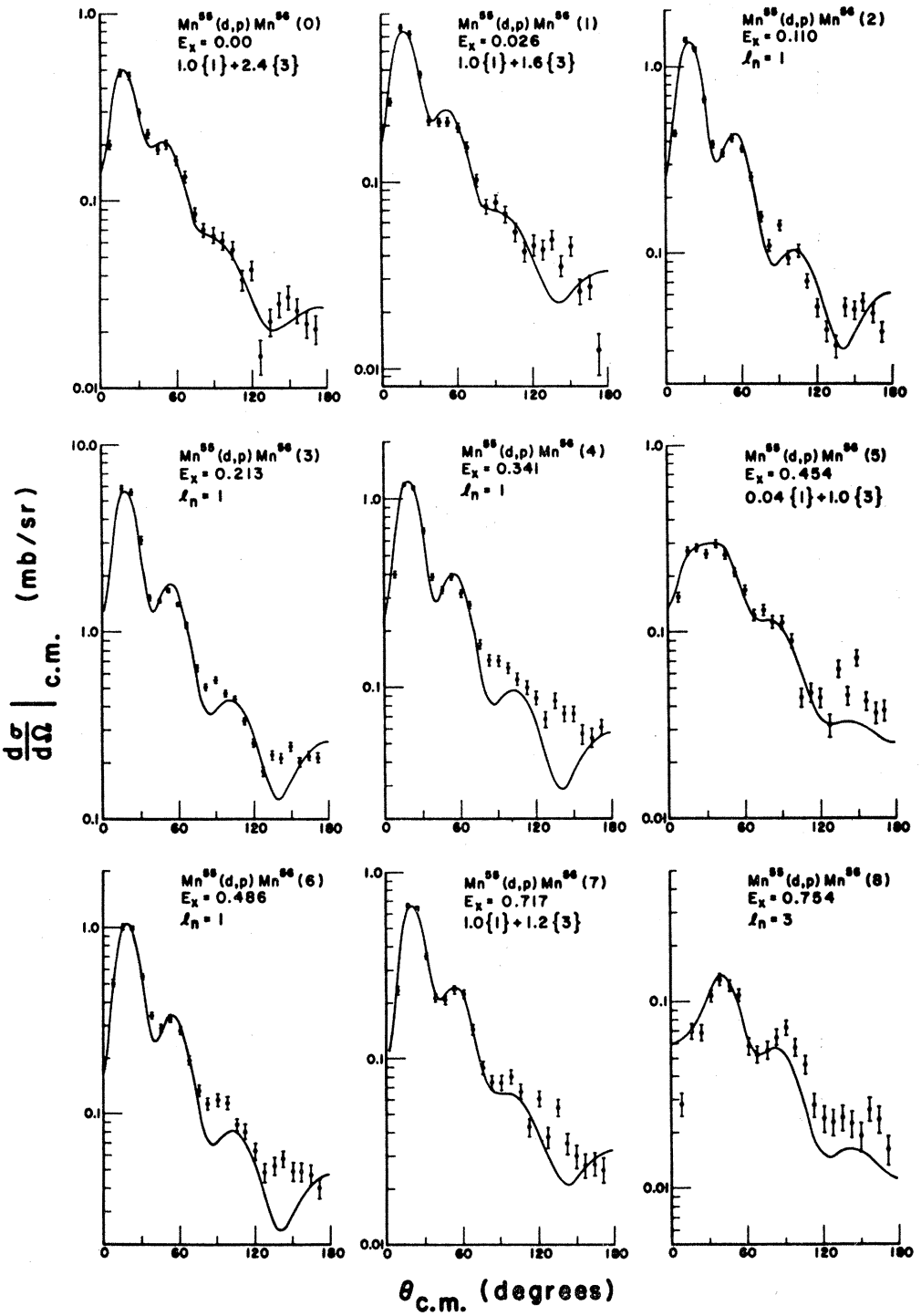

FIG. 5. Angular distributions for the lowest nine states of Mn^{56}. The curves are from DW calculations. Excitation energies E_x are listed. The coefficients are relative mixing ratios before normalization to the data. See also the caption of Fig. 4.

accurate to within about 20%. This is based on an analysis of the summed transition strengths. The accuracy for each state, particularly for the weak ones, may be worse than 20%. Those for l_n values of 0, 1, and 2 are experimentally determined more accurately than those for l_n values of 3 and 4.

IV. INTERPRETATION

A. Properties of Mn^{56} States

One of the most obvious features of the present results is the very extensive degree of configuration mixing. Most angular distributions required at least two sepa-

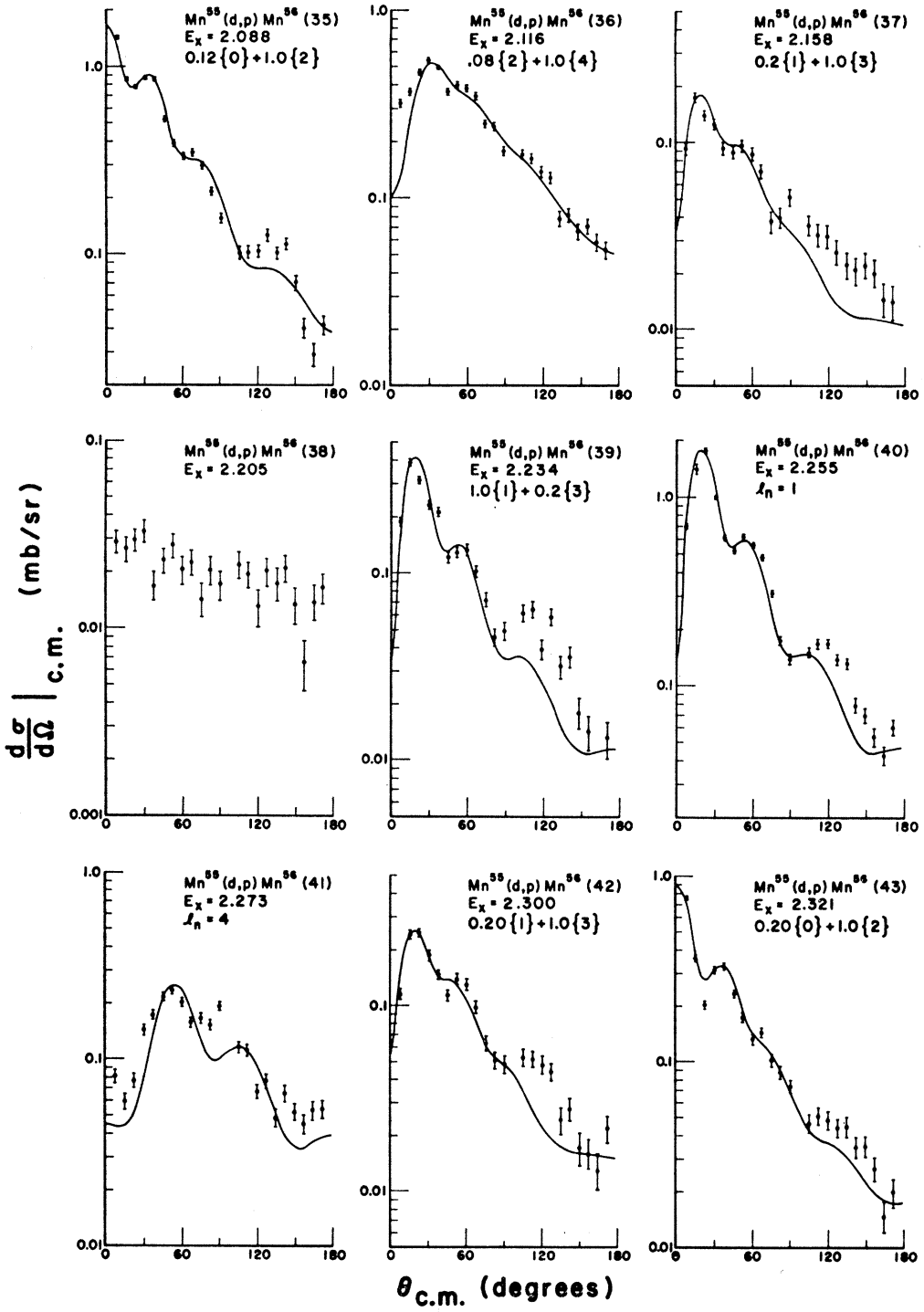

FIG. 6. Angular distributions for states 35–43. See also the captions of Figs. 4 and 5.

rate l_n components in the DW calculations. Also, the ground and first excited states of Mn^{56} have $l_n=3$ spectroscopic factors which are twice as large as those for $l_n=1$, in contrast to the expected ordering of the shell-model orbitals. These facts suggest complicated wave functions for the Mn^{56} states.

In view of the $J^\pi=\frac{5}{2}^-$ character of the Mn^{55} target, it is virtually impossible to determine the spins of the final states and, in fact, no definite assignments were made. The limits of possible spin values are restricted by the lowest l_n value in a mixed angular distribution. Thus for distributions with $l_n=0$ components, $J_f^\pi=2^-$ or 3^-, assuming normal stripping processes.

Figure 8 presents a summary of the properties of

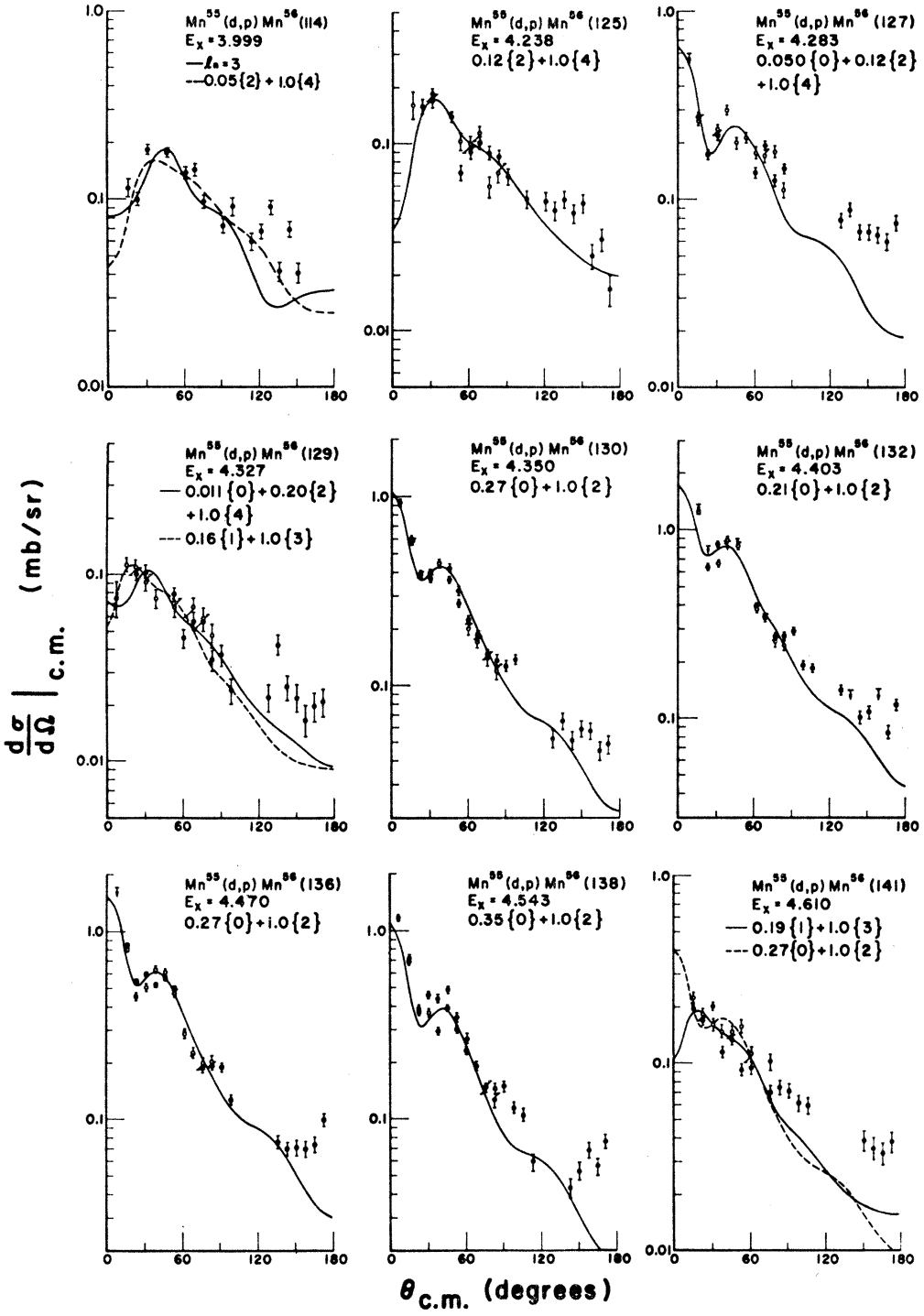

FIG. 7. Angular distributions for selected states between 3.99 and 4.61 MeV. See also the captions for Figs. 4 and 5. Solid circles and open circles represent the data for the first and second main exposures, respectively.

the low-lying states in Mn^{56}. The last three columns list the relative (n, γ) transition probabilities[43,45] and the (d, p) transition strengths $(2J_f+1)S_l$ as obtained from Table III. The arrows indicate possible electromagnetic decay transitions found in the study of the (n, γ) reaction.[43] They were assigned only the basis of energy differences and may be improperly located in the spectrum.

The spins of the lowest three states of Mn^{56} are known

[45] W. V. Prestwich (private communication).

TABLE III. Summary of experimental results for the $Mn^{55}(d, p)Mn^{56}$ reaction. For the l_n values, question marks (?) mean that a stripping pattern may be present, but that no l_n value could be assigned, and n.s. means that no stripping pattern was discernible. Parentheses enclose uncertain assignments. The notation (n, γ) means that the level is seen in the (n, γ) reaction, but not in the (d, p) reaction.

Level	E_x (MeV)	l_n	$[(2J_f+1)/(2J_i+1)]S_{lj}$	$J\pi$	$(d\sigma/d\Omega)_{max}$ (mb/sr)
0	0.000	1	0.10	3+	0.48
		+3	0.25		
1	0.026	1	0.14	2+	0.67
		+3	0.22		
2	0.110	1	0.30	1+	1.40
3	0.213	1	1.3	+	5.87
4	0.341	1	0.28	+	1.19
5	0.454	1	0.028	+	0.30
		+3	0.70		
6	0.486	1	0.22	+	1.02
7	0.717	1	0.13	+	0.66
		+3	0.15		
8	0.754	3	0.35	+	0.13
9	0.842	1	0.035	+	0.18
		+3	0.056		
10	1.166	1	0.13	+	0.70
10a	1.179	(n,γ)			
11	1.192	1	0.0037	+	0.040
		+3	0.093		
12	1.238	1	0.0076	+	0.089
		+3	0.19		
13	1.251	(n,γ)			
14	1.293	1	0.0037	+	0.038
		+3	0.073		
15	1.321	(n,γ)			
16	1.349	1	0.050	+	0.26
		+3	0.020		
17	1.376	(n,γ)			
18	1.434	(n,γ)			
19	1.486	n.s.			0.026
20	1.510	1	0.053	+	0.28
21	1.560	3	0.14	+	0.056
22	1.582	(n,γ)			
23	1.639	(n,γ)			
24	1.667	(n,γ)			
25	1.695	(n,γ)			
26	1.727	1	0.067	+	0.44
		+3	0.33		
27	1.742	1	0.14	+	0.78
		+3	0.056		
28	1.834	1	0.034	+	0.21
		+3	0.057		
29	1.865	?			0.066
30	1.949	1	0.019	+	0.10
		+3	0.063		
31	1.976	(0)	(0.0078)	−	0.80
		+2	0.20		
		+4	1.2		
32	2.015	1	0.015	+	0.10
		+3	0.037		
33	2.038	?			0.12
34	2.071	1	0.030	+	0.20
		+3	0.060		
35	2.088	0	0.030	−	1.43
		+2	0.25		
36	2.116	2	0.12	−	0.54
		+4	1.5		
37	2.158	1	0.031	+	0.17
		+3	0.16		
38	2.205	n.s.			0.033
39	2.234	1	0.063	+	0.38
		+3	0.013		
40	2.255	1	0.28	+	1.80
41	2.273	4	1.3	−	0.24
42	2.300	1	0.033	+	0.24
		+3	0.16		
43	2.321	0	0.016	−	0.75
		+2	0.080		
44	2.338	3	0.15	+	0.080
45	2.362	1	0.15	+	0.91

TABLE III (*Continued*)

Level	E_x (MeV)	l_n	$[(2J_f+1)/(2J_i+1)]S_{lj}$	$J\pi$	$(d\sigma/d\Omega)_{max}$ (mb/sr)
46	2.394	1	0.30	+	1.78
47	2.421	3	0.43	+	0.22
47a	2.432	(n,γ)			
48	2.438	3	0.17	+	0.080
49	2.474	(n,γ)			
50	2.519	n.s.			0.028
51	2.546	?			0.085
51a	2.556	(n,γ)			
52	2.580	1	0.10	+	≤0.76
		+3	0.40		
53	Unresolved doublet with level 52				
54	2.628	n.s.			0.065
55	2.653	n.s.			0.028
56	2.682	(1, +3)	(0.010, 0.033)	(+)	0.10
57	2.704	1	0.007	+	0.060
		+3	0.023		
58	2.720	1	0.050	+	0.35
		+3	0.10		
58a	2.755	(n,γ)			
59	2.780	1	0.0040	+	0.055
		+3	0.080		
60	2.798	1	0.0090	+	0.060
61	2.824	1	0.090	+	0.74
		+3	0.45		
61a	2.833	(n,γ)			
62	2.855	1	0.029	+	0.19
63	2.873	0	0.0059	−	0.29
		+2	0.027		
64	2.890	(1, +3)	(0.0087, 0.17)		0.12
		or (0, +2, +4)	(0.0011, 0.026, 0.16)		
65	2.922	1	0.017	+	0.14
		+3	0.027		
66	2.942	n.s.			0.032
67	2.951	1	0.042	+	0.32
		+3	0.070		
68	3.001	0	0.0021	−	0.10
		+2	0.023		
69	3.020	1	0.12	+	0.82
70	3.047	1	0.036	+	0.29
		+3	0.055		
71	3.075	1	0.028	+	0.20
72	3.102	(1, +3)	(0.0057, 0.14)		0.10
		or (0, +2, +4)	(0.0009, 0.021, 0.13)		
73	3.130	1	0.0086	+	0.070
		+3	0.014		
74	3.164	2	0.039	−	0.18
		+4	0.15		
75	Unresolved doublet with level 74				
76	3.220	2	0.022	−	0.11
		+4	0.19		
76a	3.229	(n,γ)			
77	3.241	1	0.097	+	0.71
77a	3.249	(n,γ)			
78	3.263	4	0.43	−	0.10
79	3.293	0	0.011	−	≤0.80
		+2	0.060		
80	3.315	?			0.046
81	3.345	n.s.			0.050
82	3.372	1	0.014	+	0.12
83	3.388	n.s.			0.070
84	3.416	1	0.018	+	0.18
		+3	0.18		
85	Unresolved doublet with level 84				
86	3.449	?			0.044
86a	3.457	(n,γ)			
87	3.466	?			0.020
88	3.488	?			0.041

TABLE III (*Continued*)

Level	E_x (MeV)	l_n	$[(2J_f+1)/(2J_i+1)]S_{lj}$	$J\pi$	$(d\sigma/d\Omega)_{max}$ (mb/sr)
89	3.500	?			0.042
90	3.525	(1)	(0.0083)	+	0.060
		or $\begin{pmatrix}1\\+3\end{pmatrix}$	$\begin{pmatrix}0.0064\\0.027\end{pmatrix}$		
91	3.544	n.s.			0.027
91a	3.568	(n,γ)			
92	3.584	1	0.021	+	0.21
		+3	0.13		
93	Unresolved doublet with level 92				
94	3.608	n.s.			0.050
95	3.627	n.s.			0.14
96	Unresolved doublet with level 95				
97	3.675	$\begin{pmatrix}2\\+4\end{pmatrix}$	$\begin{pmatrix}0.015\\0.047\end{pmatrix}$	(−)	0.075
98	3.696	1	0.012	+	0.10
		+3	0.023		
99	3.721	$\begin{pmatrix}1\\+3\end{pmatrix}$	$\begin{pmatrix}0.0054\\0.022\end{pmatrix}$	(+)	0.055
100	3.750	n.s.			0.10
101	3.766	n.s.			0.050
102	3.794	?			0.095
103	Unresolved doublet with level 102				
104	3.823	4	0.67	−	0.14
105	3.838	(4)	(0.22)	(−)	0.050
		or (n.s.)			
106	3.862	n.s.			0.027
107	3.878	?			0.19
108	Unresolved doublet with level 107				
109	3.902	n.s.			0.050
110	3.928	$\begin{pmatrix}1\\+3\end{pmatrix}$	$\begin{pmatrix}0.011\\0.028\end{pmatrix}$	(+)	0.10
111	3.959	n.s.			0.015
112	3.976	n.s.			0.032
113	3.982	n.s.			0.050
114	3.999	(3)	(0.31)		0.18
		or $\begin{pmatrix}2\\+4\end{pmatrix}$	$\begin{pmatrix}0.023\\0.47\end{pmatrix}$		
115	4.028	n.s.			0.10
116	Unresolved doublet with level 115				
117	4.072	$\begin{pmatrix}1\\+3\end{pmatrix}$	$\begin{pmatrix}0.0080\\0.080\end{pmatrix}$	(+)	0.085
118	4.099	n.s.			0.060
119	4.118	n.s.			0.080
120	4.133	n.s.			0.060
121	4.153	?			0.11
122	4.172	?			0.075
123	4.194	?			0.080
124	4.225	2	0.023	−	0.12
		+4	0.11		
125	4.238	2	0.028	−	0.18
		+4	0.23		
126	4.263	n.s.			0.050
127	4.283	0	0.011	−	<0.57
		+2	0.026		
		+4	0.21		
128	4.302	0	0.0047	−	0.21
		+2	0.023		
		+4	0.12		
129	4.327	$\begin{pmatrix}0\\+2\\+4\end{pmatrix}$	$\begin{pmatrix}0.0009\\0.017\\0.087\end{pmatrix}$		0.11
		or $\begin{pmatrix}1\\+3\end{pmatrix}$	$\begin{pmatrix}0.010\\0.063\end{pmatrix}$		
130	4.350	0	0.018	−	0.95
		+2	0.067		
131	4.374	$\begin{pmatrix}1\\+3\end{pmatrix}$	$\begin{pmatrix}0.0060\\0.050\end{pmatrix}$		0.065
		or $\begin{pmatrix}0\\+2\\+4\end{pmatrix}$	$\begin{pmatrix}0.0007\\0.012\\0.060\end{pmatrix}$		
132	4.403	0	0.028	−	1.25
		+2	0.13		

TABLE III (*Continued*)

Level	E_x (MeV)	l_n	$[(2J_f+1)/(2J_i+1)]S_{lj}$	$J\pi$	$(d\sigma/d\Omega)_{max}$ (mb/sr)
133	4.418	$\begin{pmatrix}1\\+3\end{pmatrix}$	$\begin{pmatrix}0.020\\0.057\end{pmatrix}$	(+)	0.20
134	4.432	?			0.080
135	4.457	n.s.			0.075
136	4.470	0 +2	0.025 0.093	−	≤1.70
137	4.512	$\begin{pmatrix}1\\+3\end{pmatrix}$	$\begin{pmatrix}0.0088\\0.11\end{pmatrix}$		0.15
		or $\begin{pmatrix}0\\+2\\+4\end{pmatrix}$	$\begin{pmatrix}0.0012\\0.022\\0.11\end{pmatrix}$		
138	4.543	0 +2	0.019 0.053	−	1.18
139	4.565	?			0.092
140	4.581	$\begin{pmatrix}0\\+2\end{pmatrix}$	$\begin{pmatrix}0.0049\\0.014\end{pmatrix}$		0.18
		or $\begin{pmatrix}1\\+3\end{pmatrix}$	$\begin{pmatrix}0.015\\0.019\end{pmatrix}$		
141	4.610	$\begin{pmatrix}1\\+3\end{pmatrix}$	$\begin{pmatrix}0.016\\0.087\end{pmatrix}$		0.22
		or $\begin{pmatrix}0\\+2\end{pmatrix}$	$\begin{pmatrix}0.0068\\0.025\end{pmatrix}$		
142	4.628	1 +3	0.035 0.035	+	0.37
143	4.643	2 +4	0.070 0.14	−	0.46
144	4.653	?			0.15
145	4.673	2 +4	0.078 0.26	−	0.50
146	4.697	n.s.			0.067
147	4.712	1 +3	0.012 0.050	+	0.15
148	4.738	1 +3	0.022 0.045	+	0.22
149	4.753	n.s.			0.066
150	4.767	1 +3	0.011 0.050	+	0.14
151	4.798	1 +3	0.040 0.13	+	0.46
152	4.809	?			0.12
153	4.819	1 +3	0.023 0.033	+	0.24
154	4.834	2 +4	0.0037 0.011	−	0.11
155	4.840	?			0.12
156	4.863	0 +2	0.010 0.040	−	0.44
157	4.886	0 +2	0.0080 0.027	−	0.35
158	4.898	n.s.			0.087
159	4.918	n.s.			0.082
160	4.927	1 +3	0.032 0.13	+	0.28
161	4.950	$\begin{pmatrix}0\\+2\end{pmatrix}$	$\begin{pmatrix}0.0051\\0.025\end{pmatrix}$		0.18
		or $\begin{pmatrix}1\\+3\end{pmatrix}$	$\begin{pmatrix}0.018\\0.030\end{pmatrix}$		
162	4.968	1 +3	0.040 0.050	+	0.40
163	4.978	n.s.			0.11
164	4.989	$\begin{pmatrix}0\\+2\end{pmatrix}$	$\begin{pmatrix}0.012\\0.060\end{pmatrix}$		0.48
		or $\begin{pmatrix}1\\+3\end{pmatrix}$	$\begin{pmatrix}0.037\\0.19\end{pmatrix}$		
165	5.013	0 +2	0.0096 0.032	−	0.32
166	5.044	2 +4	0.032 0.080	−	0.20
167	5.065	0 +2	0.0054 0.018	−	0.17
168	5.072	$\begin{pmatrix}2\\+4\end{pmatrix}$	$\begin{pmatrix}0.045\\0.18\end{pmatrix}$		0.38
		or $\begin{pmatrix}1\\+3\end{pmatrix}$	$\begin{pmatrix}0.026\\0.087\end{pmatrix}$		

TABLE III (*Continued*)

Level	E_x (MeV)	l_n	$[(2J_f+1)/(2J_i+1)]S_{lj}$	$J\pi$	$(d\sigma/d\Omega)_{max}$ (mb/sr)
169	5.085	?			0.18
170	5.113	2	0.023	−	0.16
		+4	0.11		
171	5.130	2	0.019	−	0.15
		+4	0.16		
172	5.161	?			0.18
173	5.172	?			0.089
174	5.188	0	0.0048	−	0.16
		+2	0.012		
175	5.208	(1 / +3)	(0.015 / 0.038)		0.18
		or (2 / +4)	(0.023 / 0.11)		
176	5.223	?			0.082
177	5.261	2	0.047	−	0.34
		+4	0.19		
178	5.275	n.s.			0.058
179	5.297	2	0.027	−	0.20
		+4	0.19		
180	5.312	2	0.037	−	0.26
		+4	0.18		
181	5.332	1	0.011	+	0.12
		+3	0.022		
182	5.343	2	0.026	−	0.22
		+4	0.17		
183	5.364	2	0.032	−	0.23
		+4	0.13		
184	5.387	?			0.074
185	5.407	2	0.033	−	0.23
		+4	0.17		
186	5.416	?			0.10
187	5.430	n.s.			0.11
188	5.445	(2 / +4)	0.042 / 0.17		0.31
		or (1 / +3)	0.025 / 0.083		
189	5.456	n.s.			0.068
190	5.471	2	0.018	−	0.16
		+4	0.090		
191	5.486	2	0.020	−	0.14
		+4	0.080		
192	5.515	?			0.17
193	5.525	n.s.			0.19
194	5.551	(2 / +4)	(0.018 / 0.073)		0.14
		or (1 / +3)	(0.012 / 0.040)		
195	5.562	n.s.			0.11
196	5.595	?			0.19
197	5.605	n.s.			0.11
198	5.642	n.s.			0.12
199	5.656	n.s.			0.12
200	5.683	n.s.			0.080
201	5.715	n.s.			0.088
202	5.733	n.s.			0.086
203	5.751	n.s.			0.048
204	5.765	n.s.			0.10
205	5.775	n.s.			0.25
206	5.797	n.s.			0.093
207	5.833	n.s.			0.17
208	5.861	n.s.			0.17
209	5.958	n.s.			0.20
210	6.266	n.s.			0.18
211	6.309	n.s.			0.19
212	6.367	n.s.			0.15
213	6.411	n.s.			0.12
214	6.464	n.s.			0.12
215	6.478	n.s.			0.12
216	6.512	n.s.			0.25
217	6.532	n.s.			0.14

from atomic-beam experiments,[46] (n, γ) reaction studies,[47,48] and study of the β decay[49] of Cr^{56}. The present experiment, however, presents a problem involving the configuration of the $J^\pi=1^+$ level at 110 keV. Assuming that there are no $p_{3/2}$ or $p_{1/2}$ proton admixtures in the wave functions, the small logft value of 4.3 for the β decay of Cr^{56} to this level suggests[49] a large $(1f_{5/2})^2$ neutron admixture in the Cr^{56} ground state, and consequently a large $1f_{5/2}$ neutron admixture in the 110-keV state of Mn^{56}. This should be seen with an $l_n=3$ transition in the (d, p) reaction. In contrast to this, the data are consistent with a pure $l_n=1$ $(p_{3/2})$ transition. However, a 25% admixture of an $l_n=3$ component would be undetectable. Further experimental investigation is required.

The 213-keV state also presents some difficulties. It decays to all three of the lower states and the multipolarity of the ground-state transition is predominantly $M1$.[47,48] It appears that only a $J^\pi=2^+$ assignment is possible for this state.

On the other hand, there are arguments supporting a $J^\pi=4^+$ assignment for this level. In view of the $2J_f+1$ factor in the transition amplitude, one might qualitatively expect such a level to be very strongly populated in the (d, p) reaction. The 213-keV level is, in fact, the most strongly populated state observed in the present experiment. Further evidence was suggested by Prestwich and Coté[50] from a study of the $Mn^{55}(n, \gamma)Mn^{56}$ reaction at thermal and resonance energies. The observed disappearance of the 213-keV level in the spectrum for the 336-eV resonance $(J^\pi=2^-)$ could then be attributed to a selection rule if the level had $J^\pi=4^+$.

The most reasonable conclusion is that the 213-keV state has $J^\pi=2^+$. If the spin were 4, an $M3$ transition would be required in the decay to the 1^+ level at 110 keV. This would not be able to compete strongly with an $M1$ transition to the ground state. The (n, γ) result for the 336-eV resonance would then have to be attributed to a small γ-ray decay width, a statistical fluctuation of a Porter-Thomas strength distribution.[51] [*Note added in proof*: Recent data (P. H. M. Van Assche, private communication) indicates that both the 213- and 341-keV levels are doublets, separated by 3 keV and 5 keV, respectively.]

A transfer of an $f_{5/2}$ neutron should populate states with $J^\pi=0^+$–5^+. Of these, only the 0^+ and 5^+ members could not also be reached with $l_n=1$ transfers. Assuming s-wave capture and $E1$ radiative decay, these members should not be populated with the (n, γ) reaction either. The levels at 454 and 754 keV satisfy these conditions and are given the tentative assignments of $J^\pi=0^+$ or 5^+. The 454-keV state does have a small (5%) admixture of an $l_n=1$ component. This might be attributed to a second-order stripping process such as, for example, target excitation to the $\frac{7}{2}^-$ level at 125 keV in Mn^{55} followed by a $p_{3/2}$ transfer. Such an interpretation conflicts with the theoretical expectations of Penny,[36] but agrees with experimental evidence of Bock *et al.*[52] If this mechanism is properly assessed, then only the $J^\pi=5^+$ assignment is possible. This is in agreement with the observed population intensity, since the

TABLE IV. Spectroscopic factors for the lowest four states of Mn^{56}.

Level	E_x (MeV)	J^π	l_n	S_l
0	0.000	3^+	1	0.089
			3	0.21
1	0.026	2^+	1	0.17
			3	0.27
2	0.110	1^+	1	0.61
3	0.213	$(2)^+$	1	(1.5)
		or $(4)^+$	1	(0.85)

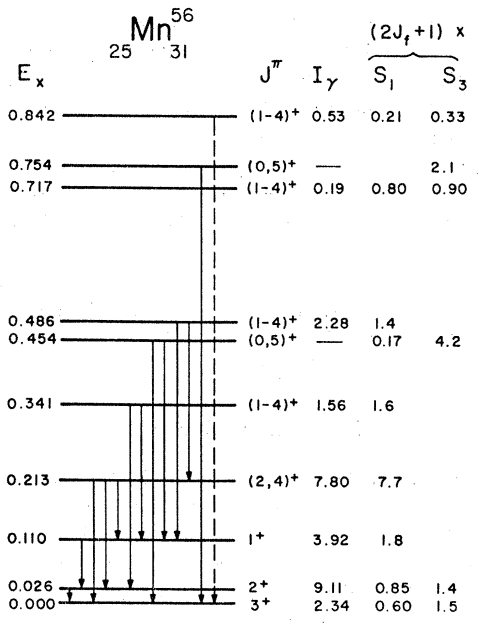

FIG. 8. Properties of the levels below 1 MeV of Mn^{56}. The J^π assignments are discussed in the text. The values for $(2J_f+1)\,S_l$ ($l_n=1$ and 3) are taken from Table III. The relative (n, γ) transition intensities I_γ are taken from Ref. 43 (the values for the 0.717- and 0.754-MeV levels are reversed in accordance with Ref. 45).

[46] W. J. Childs, L. S. Goodman, and L. J. Kieffer, Phys. Rev. **122**, 891 (1961).
[47] N. D'Angelo, Phys. Rev. **117**, 510 (1960).
[48] I. V. Estulin, A. S. Melioransky, and L. F. Kalinkin, Nucl. Phys. **24**, 118 (1961).
[49] B. J. Dropesky, A. W. Schardt, and T. T. Shull, Nucl. Phys. **16**, 357 (1960).
[50] W. V. Prestwich and R. E. Coté, Phys. Rev. **155**, 1223 (1967).
[51] C. E. Porter and R. G. Thomas, Phys. Rev. **104**, 483 (1956).
[52] R. Bock, H. H. Duhm, R. Rüdel, and R. Stock, Phys. Letters **13**, 151 (1964).

$J^\pi=0^+$ choice leads to a seemingly large spectroscopic factor of $S_3=4.2$. However, the state apparently decays to both 3^+ and 1^+ levels with comparable intensities.[43] A $J^\pi=0^+$ assignment does not improve the situation. Similar remarks apply to the 754-keV state.

There is an interesting group of levels in Mn^{56} which are populated with the thermal (n, γ) reaction, but not with the (d, p) reaction. This is surprising, since the latter reaction has less stringent restrictions on the transition amplitude, unless the target is not a good parent of the final state. Such states can be reached with the (n, γ) reaction if a complex compound-nucleus state is formed in the process.

B. Reaction Mechanisms

The present data were compared with data from the $Mn^{55}(n, \gamma)Mn^{56}$ reaction[43,50] in an earlier publication.[13] It is also interesting and important to investigate the (d, p) reaction mechanism and to assess the reliability of the DW analysis. This is most conveniently done with the (d, p) sum rule[53]

$$\sum_{(i)} [(2J_f^{(i)}+1)/(2J_i+1)]S_l^{(i)}=N_l, \qquad (5)$$

where N_l is the number of holes in the l_n shell-model orbital of the target nucleus. The sum extends over all states which have the same l_n. In the application of this expression, it must be assumed that all of the available single-particle strength has been detected and that the Q dependence of the reaction is properly given by the DW calculations.

Figure 9 presents the observed strength function for the $Mn^{55}(d, p)Mn^{56}$ reaction. The $l_n=1$ strength function shows two regions of prominent strength: near 0.0–0.5 and near 2.0–2.5 MeV. The strength is quite small outside of these regions and appears to vanish entirely near 4 MeV. There is some additional strength near 4.5–5.0 MeV. Although this may belong to the $3p$ orbitals, we shall assume that it can rather be associated with the $2p$ orbitals. The $l_n=3$ strength function does not show any particular region of dominance. There are definite indications that it is beginning to vanish above 5 MeV. The behavior of the strength functions strongly suggests that nearly all of the available $2p_{3/2}$, $2p_{1/2}$, and $1f_{5/2}$ strengths have been detected.

The transition strengths listed in Table III have been summed for each value of l_n and the totals are given in Table V. The minimum sums correspond to the shaded bars of Fig. 9, while the maximum sums include the open bars. All totals have been reduced by 20% from the actual sums obtained from Table III in accordance with the finite-range and nonlocality corrections of Table II. In addition, the sums for $l_n=3$ and 4 have been modified in accordance with the neutron spin-orbit corrections of Table II, assuming $f_{5/2}$ and $g_{9/2}$ transfers, respectively. In the right-hand columns are listed the maximum values expected for the sums, based on the assumption that the Mn^{55} ground state has a $p_{3/2}^2$ neutron configuration.

It is seen that the $l_n=1$ and $l_n=3$ sums are very close to, but slightly in excess of, their expected values. The discrepancies are near to or less than 20% and suggest that the DW calculations are reliable to approximately this degree of accuracy. The sums are consistent with the assumption that the Mn^{55} ground state has a $p_{3/2}^2$ neutron configuration but, within the accuracy of the experiment, admixtures of the $f_{5/2}$ orbital are not precluded.

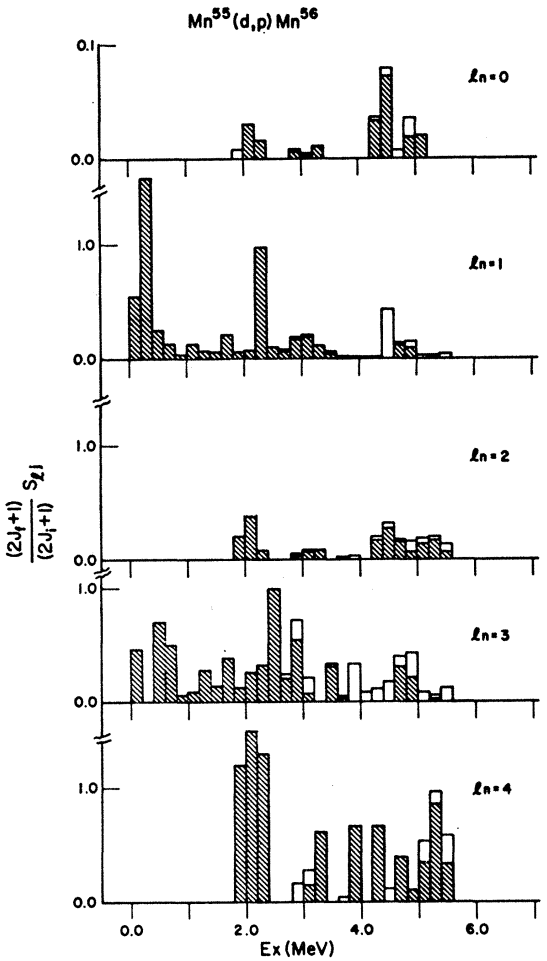

FIG. 9. The $Mn^{55}(d, p)Mn^{56}$ strength function. The transition strengths from Table III are summed in 200-keV intervals and plotted as a histogram against excitation energy for each value of l_n. The shaded bars represent certain l_n assignments and the open bars represent additional amounts for uncertain assignments of l_n. There is some duplication of the open bars between different values of l_n.

[53] M. H. Macfarlane and J. B. French, Rev. Mod. Phys. **32**, 567 (1960).

TABLE V. Summed transition strengths for the $Mn^{55}(d, p)Mn^{56}$ reaction for each value of observed l_n. Shell-model theoretical limits based on a $(2p_{3/2})^2$ neutron configuration of Mn^{55} are also given. See text and the caption of Fig. 9 for the meaning of minimum and maximum.

	$[(2J_f+1)/(2J_i+1)]S_{lj}$		Shell model	
l_n	Min.	Max.	Orbitals	Sum limit
0	0.166	0.200	$3s_{1/2}$	2.0
1	4.01	4.55	$2p_{3/2}+2p_{1/2}$	4.0
2	1.49	1.80	$2d_{5/2}+2d_{3/2}$	10.0
3	5.96	7.63	$1f_{5/2}$	6.0
4	5.25	6.43	$1g_{9/2}$	10.0

V. NUCLEAR MODELS

A. Statistical Model

With over 200 levels known in Mn^{56} up to 6 MeV of excitation energy, it is possible and convenient to compare their number, energy distribution, and nearest-neighbor spacings with the predictions of the statistical model.

At low excitation energies, the number of levels $N(E)$ below the excitation energy E is given by the phenomenological expression[54]

$$N(E)=\exp[(E-E_0)/T]. \quad (6)$$

The parameter T is called the nuclear temperature and E_0 is a type of condensation energy related to the nuclear pairing energy. It is negative for odd-odd nuclei. The nuclear level density $\rho(E)$ is given by

$$\rho(E)=dN(E)/dE=T^{-1}\exp[(E-E_0)/T]=T^{-1}N(E). \quad (7)$$

At higher energies (above the first few MeV of excitation), in the region more suitable to statistical techniques, theoretical expressions can be derived for the level density.[55,56] Techniques are available for matching the formulas between the different regions.[56]

Theoretical expressions for the nearest-neighbor spacings of energy levels are also available. If s is the spacing between two adjacent levels and D is the average spacing in the region, then the distribution for states with the same spin and parity is given[57] by the Wigner expression

$$\rho(s)=\tfrac{1}{2}\pi(s/D)\exp(-\pi s^2/4D^2). \quad (8)$$

The spacing distribution for randomly distributed levels of all spins and parities is expected to be approximately exponential[58]:

$$\rho(s)\propto\exp(-s/D). \quad (9)$$

A semilogarithmic plot of $N(E)$ against E is presented in Fig. 10. According to Eq. (6), the data should approximate a straight line. Two sets of data are shown in the figure. The lower set was taken from the MIT measurements of level positions.[15] The upper set was taken from Table III. It includes all the levels seen in this (d, p) experiment, supplemented with a few levels seen only by the (n, γ) reaction[43] within the region labeled (n, γ). Without any additional information it would be very difficult to draw a relaible straight line through the upper set of data.

In this regard, it is instructive to consider the level density. According to Eq. (7), it should have the same dependence as $N(E)$ on the energy E. Figure 11 illustrates the data. The level density, in levels per MeV, was obtained by counting the number of levels listed in Table III in 500-keV intervals and multiplying by 2. Again, it would be difficult to draw a reliable straight line through the data, particularly above 3 MeV.

There is, however, an independent item of information. The level density of $J^\pi=2^-$ and 3^- levels at the neutron binding energy is known[59] from the scattering of low-energy (s-wave) neutrons from Mn^{55}. The average level spacing is $D_{res}=2.1\pm0.7$ keV (as quoted by Gilbert and Cameron[56]) or the level density is $\rho_{res}=480$ MeV^{-1}. (The recent data of Rohr and Friedland[60] are in agreement with these values, yielding $D_{res}\approx1.9$ keV.) This is shown as the circle in Fig. 11. By using the theoretical expressions for level density,[56] one can calculate the density for levels of all spin and parity. This is shown as the square point in Fig. 11.

The level density of Mn^{56} has been calculated from Eq. (7) and the parameters given by Gilbert and Cameron.[56] It is shown as line 1 in Figs. 10 and 11. The calculation is correct up to the matching energy of 4.6 MeV. Above that energy the correct line would slowly curve away from line 1 and pass through the square point of Fig. 11. It does not differ significantly from line 1 in the region of interest. The parameters for

[54] T. Ericson, Nucl. Phys. **11**, 481 (1959).
[55] T. Ericson, Advan. Phys. **9**, 425 (1960).
[56] A. Gilbert and A. G. W. Cameron, Can. J. Phys. **43**, 1446 (1965).
[57] P. B. Kahn and C. E. Porter, Nucl. Phys. **48**, 385 (1963).
[58] N. Rosenzweig and C. E. Porter, Phys. Rev. **120**, 1698 (1960).
[59] R. E. Coté, L. M. Bollinger, and G. E. Thomas, Phys. Rev. **134**, B1047 (1964).
[60] G. Rohr and E. Friedland, Nucl. Phys. **A104**, 1 (1967).

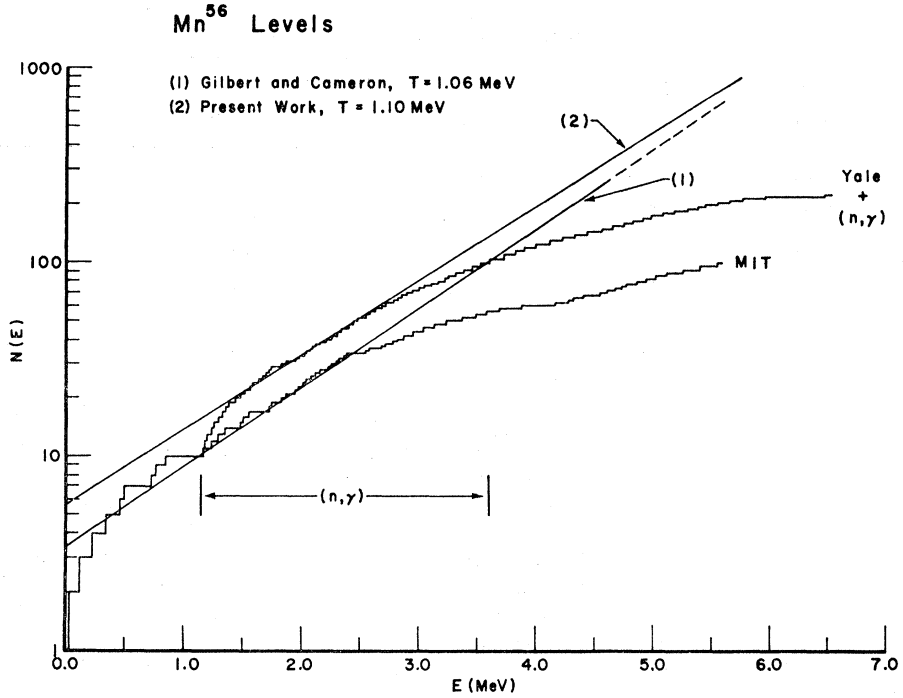

FIG. 10. Number of levels $N(E)$ below the excitation energy E plotted against E. See text for a description of the data and the lines labeled 1 and 2.

line 1 were obtained from an analysis of the MIT data and the line clearly fits that data quite well.

The line which is consistent with the present experimental data, line 2, was obtained in the following manner. It was assumed that the level density could be represented by a straight line in Fig. 11 all the way to the neutron binding energy and that it would intersect line 1 at that energy. It was also assumed that the level density at $E=2.25$ MeV was exactly $\rho=38$ MeV^{-1}. These two points determined the straight line marked 2 in Fig. 11. This line was also superimposed onto Fig. 10 in accordance with Eq. (7), and the parameters $T=1.10$ MeV and $E_0=-2.0$ MeV were obtained. It is seen that line 2 fits the data quite well, particularly in the region between 1.5 and 3.0 MeV.

The failure of line 2 in Figs. 10 and 11 to follow the

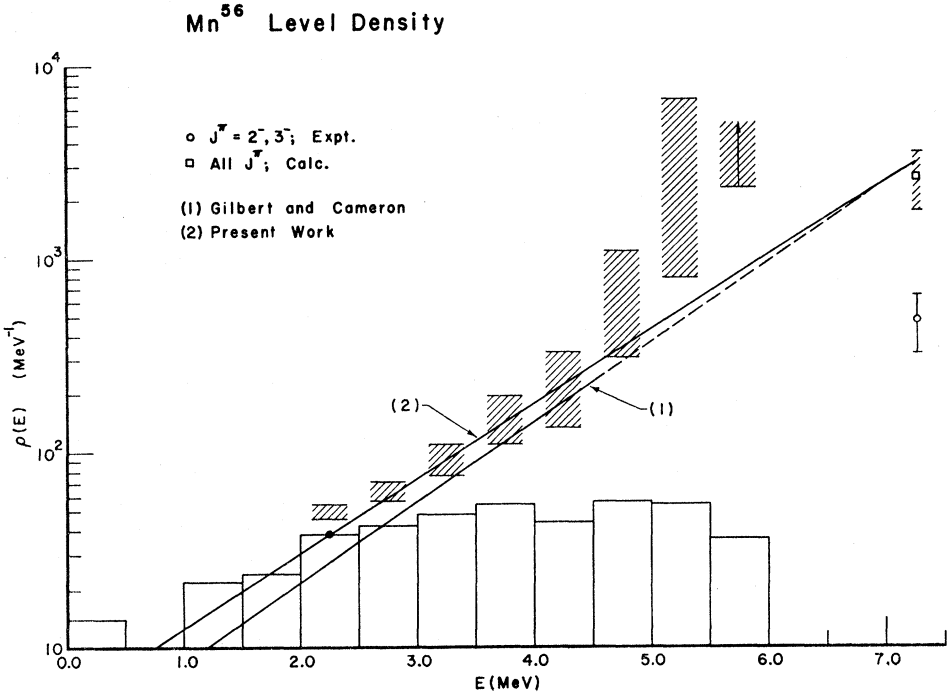

FIG. 11. Plot of the observed level density against excitation energy. Also shown is the density of levels at the neutron binding energy as determined from neutron scattering experiments (see also text). See text for a description of lines 1 and 2 and the shaded regions.

data above 3 MeV is due partly to the failure of the (d, p) reaction to populate all the possible states and partly to the finite resolution of the apparatus. We may correct for the latter if we assume that the nearest-neighbor spacings have an exponential distribution, Eq. (9). We suppose that adjacent levels with spacings less than $\Delta E_1=5$ keV could not be experimentally resolved and that adjacent levels with spacings greater than $\Delta E_2=9$ keV could always be resolved. Then the limits on the corrected value of the level density ρ_{cor} are given by

$$\rho_{obs}\exp(\Delta E_1/D)<\rho_{cor}<\rho_{obs}\exp(\Delta E_2/D). \quad (10)$$

The values of the average level spacing D were taken as the reciprocals of the level densities as given by line 2 at the mean energy of each region. The acceptable values of ρ_{cor} are indicated by the shaded regions above the bars of the histogram in Fig. 11. They are not shown below 2 MeV because they are not statistically significant there.

The shaded regions in Fig. 11 are thus measures of the consistency of line 2 with the observed data. There is excellent agreement below 5 MeV. Between 5 and 6 MeV, however, the shaded regions diverge quite significantly from line 2. The most reasonable explanation for this is that the distribution of level spacings is not exponential, but retains some of the features of the Wigner distribution, Eq. (10). This is at variance with very recent evidence obtained from the analysis of nearly 1000 levels in medium-mass nuclei.[61]

It is clear from Fig. 10 that nearly all levels have been detected below 3 MeV. However, even though data for 200 levels below 6 MeV have been obtained and analyzed, there are apparently an additional 800 levels which remain undetected. Hopefully, in view of our treatment of backgrounds, these have very little single-particle strength and do not affect previous discussions.

B. Shell Model

Only very qualitative information can be obtained about the shell model from the present experimental results. The strength functions shown in Fig. 9 can be used to estimate the locations of the neutron single-particle orbits. It must be kept in mind that for some of the l_n values, both values of j_n can have significant strength and that these cannot be distinguished. Furthermore, not all of the available strength has been detected for the even values of l_n.

The $l_n=1$ strength function shows two regions of prominence: one near 0.3 MeV and one near 2.4 MeV. Since the shell-model splitting between the $p_{3/2}$ and $p_{1/2}$ orbitals is expected to be about 2.5 MeV,[1] it is tempting to assign these orbitals to the first and second prominences, respectively. However, the extensive configuration mixing known to be present argues against such a simple association.

Schiffer, Lee, and Zeidman[16] have examined the $Mn^{55}(d, p)Mn^{56}$ reaction with very broad energy resolution for the purpose of determining the regions of the shell-model orbitals. Prominent $l_n=1$ strength was found near excitation energies of 0.5 and 2.0 MeV, which were attributed to $p_{3/2}$ and $p_{1/2}$ transitions, respectively. The $2d_{5/2}$ orbital ($l_n=2$) was assigned near 2.8 MeV and the $3s_{1/2}$ orbital ($l_n=0$) was assigned near 4.7 MeV. The measurements of Dalton *et al.*[17] indicated that there was some ambiguity in these assignments. The present measurements show that the locations of the $l_n=1$ prominences are roughly correct, but the association with the $p_{3/2}$ and $p_{1/2}$ orbitals is not clear. The region of $l_n=0$ strength was correctly identified, but this cannot be taken as the location of the $3s_{1/2}$ orbital, since only $\frac{1}{10}$ of the available strength has been detected. Their location of the $l_n=2$ strength is quite inconsistent with the present data, which show prominent strength near 2.0 and 5.0 MeV, but none at 2.8 MeV.

The detailed comparison of the Mn^{56} spectrum with shell-model calculations is extremely difficult, since none has been done specifically for this nucleus. It is unlikely that realistic calculations will be available for some time, since it is clear that, as a minimum, the neutron orbitals $2p_{3/2}$, $2p_{1/2}$, and $1f_{5/2}$ must all be included together. The comparison would also be weakened by the limited knowledge of the spins of the Mn^{56} states.

C. Deformed Model

A large degree of configuration mixing implies that the nuclear residual interactions are quite strong and that the angular momenta l and j are not good quantum numbers. This raises both practical and theoretical difficulties for spherical shell-model calculations. Although such calculations are not prohibited, it is frequently more reasonable and convenient to assume that the nuclear potential is deformed. We shall now suggest that a deformed basis may be a quite realistic assumption for Mn^{56}.

It would not be entirely surprising if Mn^{56} has a large static deformation. The ground state of Mn^{55} has $J=\frac{5}{2}$. This is not consistent with the extreme single-particle model and requires special coupling arrangements of the five $f_{7/2}$ protons in more sophisticated forms of the shell model. Furthermore, the electric quadrupole moment of Mn^{55} has a rather large value of $Q=0.55$ b. This is very difficult to reproduce, even in shell-model calculations which include large amounts of configuration mixing.[62]

As was the case with the shell model, very few deformed-model calculations exist for Mn^{56}. Calculations have recently been made with the Coriolis coupling

[61] J. R. Huizenga and A. A. Katsanos, Nucl. Phys. A98, 614 (1967).

[62] E. H. Schwarz, Phys. Rev. 129, 727 (1963).

model and a Nilsson basis[6,7] for several odd-mass nuclei in the vicinity of the $1f_{7/2}$ shell. They suggest that these nuclei may have large static deformations. The techniques are being extended to treat odd-odd nuclei and preliminary calculations have been made[12] for Mn^{56}. For large negative deformations, the calculated density below 1 MeV and the location of the few states whose spins are known are in general agreement with the experimental results. The calculated level density is much too large at other deformations. One possible limitation of these calculations is the prediction of a low-lying $J^\pi=4^+$ level. The experimental counterpart of this has not been positively identified. It can only be hoped that further experimental and theoretical efforts will shed more light on the nature of Mn^{56}.

VI. SUMMARY AND CONCLUSIONS

It is abundantly clear that Mn^{56} is an exceptionally complicated nucleus and that many problems remain to be solved. The extensive degree of configuration mixing not only illustrates the complexity, but also prevents realistic calculations (at least with the shell model) from being done readily. There is some hope that calculations with the deformed model[12] may be more informative.

In spite of the voluminous data which were presented here, many of the properties of the Mn^{56} states are still unknown. No new spin assignments were made and even the few suggestions that could possibly be made were subject to severe objections. The problems are generally created by the possible decay γ rays shown in Fig. 8. These may not be correctly located and their verification is required.

A further problem is associated with the configuration of the 110-keV state. Within the framework of the simple shell model, the fast β decay of Cr^{56} to this state and the absence of an $l_n=3$ (d, p) transition are not compatible. Admixtures of the neutron $1f_{5/2}$ orbital in the ground states of Cr^{56} and Mn^{55} are suggested.

Success, however, was apparently achieved with the DW calculations of the angular distributions. The shapes were reproduced quite well and the summed spectroscopic strengths agreed with the expected shell-model values within about 20%. The theoretical sums are model-dependent and one should keep in mind that the experimental values for $l_n=0$, 1, and 2 are more accurately determined than those for $l_n=3$ and 4.

Further success was achieved in the comparison with the statistical model. This model gave a good description of the number of levels and their density as a function of excitation energy. However, an analysis of the nearest-neighbor spacings revealed that the exponential distribution expected for levels of all spins and parity was not consistent with the present data. Features of the Wigner distribution were evident. This conflicts with recent evidence,[61] but the problem is far from solved.

Comparison with nuclear-structure models must ultimately depend on an increased set of spin assignments for the Mn^{56} states. Several experiments can be proposed. It is imperative, first of all, that the decay γ rays be correctly identified in the spectrum. The $Mn^{55}(d, p\gamma)Mn^{56}$ and $Mn^{55}(n, \gamma\gamma)Mn^{56}$ reactions, with coincidences required between the outgoing reaction products, can accomplish this. Internal conversion coefficients would also help. Finally, two-particle transfer reactions on even nuclei, such as $Cr^{54}(He^3, p)Mn^{56}$ and $Fe^{58}(d, \alpha)Mn^{56}$, would also greatly aid in identifying the characteristics of the Mn^{56} states. It is hoped that theoretical techniques for calculating the spectra of such complex nuclei will develop along with the experimental data.

ACKNOWLEDGMENTS

This work has greatly benefitted from the advice and criticism of many friends and colleagues. In particular, Professor C. K. Bockelman has contributed much insight and inspiration. Dr. R. H. Siemssen also provided generous help and guidance. The experiment was accomplished with the cooperation of Dr. H. Enge and the tireless assistance of A. Sperduto. The photographic plates were carefully scanned by C. Vanegas, L. Simmons, and I. Kikuchi. Dr. J. Erskine kindly provided us with program AUTOFIT. Some of the calculations were done at the New York University Computer Center.